RESEARCH ARTICLE

SYNTHESIS AND CHARACTERIZATION OF BIMETALLIC MAGNETITE NANOPARTICLES (FE–CU, FE–AG, FE–ZN) FOR DECOLORIZATION OF SYNTHETIC DYES

MD FEDAUL MUSTAFA[1], Dr. Mansi Mishra[2], Dr. Sujeet Singh[3]

[1]*Department of Biotechnology, Noida Institute of Engineering and Technology, Greater Noida,* mdfedaulmustafa28@gmail.com

[2]*Department of Biotechnology, Noida Institute of Engineering and Technology, Greater Noida, mansi.mishra@niet.co.in*

[3]*Department of Biotechnology, Noida Institute of Engineering and Technology, Greater Noida, sujeetkumar@niet.co.in,*

Corresponding Author: *mdfedaulmustafa28@gmail.com*

Received: 25th June 2026; **Revised:** 28th July 2026; **Accepted:** 10th October 2026; **Available Online:** 15th October 2026

Abstract

The Toxicity, low biodegradability and carcinogenicity of synthetic dyes released from textile factories, paper industry, leather industry and printing companies create an environmental challenge. Decolorization technique that uses magnetic nanoparticles has an attractive feature of high surface-to-volume ratio, adjustable surface chemistry and simple recovery of used catalyst. In this study magnetite (Fe_3O_4) nanoparticles and three bimetallic types, which are Fe–Cu, Fe–Ag and Fe–Zn, were created by chemical co-precipitation method and tested for decolorization of methylene blue (MB), a kind of cationic dye. Characterization of the synthesized materials was performed by means of X-ray diffraction (XRD), scanning electron microscopy (SEM), transmission electron microscopy (TEM), Fourier-transform infrared spectroscopy (FTIR) and ultraviolet-visible spectroscopy (UV–Vis). Batch decolorization was observed based on the contact time, amount used, initial concentration of dye and pH. The reusability was also assessed for five rounds. Fe–Cu provided the highest decolorization efficiency (98.4%) at concentration (0.8 g/L), pH 9- and 90 min of contact time. Other materials such as Fe–Ag (95.2%), Fe–Zn (91.0%) and Fe_3O_4 (82.5%) performed lower than Fe–Cu. The kinetics of all four materials were best fitting the pseudo-second kinetic model ($R^2 > 0.99$), which is also indicative of the rate controlling mechanism being chemisorption step. Fe–Ag has the highest reusability at 92.1% after five rounds of recycling. Thus, the study illustrates clear structure-activity relationships, revealing Fe–Cu to be the most efficient material and Fe–Ag having the highest reusability.

Keywords: Adsorption kinetics, Bimetallic nanoparticles, Co-precipitation, Dye decolorization, Fe–Ag, Fe–Cu, Fe–Zn, Magnetite nanoparticles, Methylene blue, Wastewater treatment

How to cite this article: Mustafa MF, Mishra M, Singh S., Synthesis and Characterization of Bimetallic Magnetite Nanoparticles (Fe–Cu, Fe–Ag, Fe–Zn) for Decolorization of Synthetic Dyes. Int J Drug Deliv Technol. 2026;16(87s): 1927-1941; DOI: 10.25258/ijddt.16.87s.208

Source of support: XX

Conflict of interest: XX

1. Introduction

The process of fast industrialization and the expansion of industries involving textiles, dyeing, printing, paper making, leather and drugs has caused the release of synthetic dyes to water ecosystems on a large scale [1]. A big part of the dyes introduced in the process of textile production is lost while dyeing and flows into wastewaters without proper treatment [3]. Dyes are able to color water intensely, even in small amounts, block light penetration and photosynthesizing processes in the water and many azo and thiazine dyes have been shown to be dangerous for marine life and the human body [2,4]. The traditional methods of treatment involve various conventional methods like coagulation-flocculation, adsorption of activated

carbon, membrane filtration and biological methods [5]. However, all these methods have a lot of drawbacks such as high treatment costs, generation of a lot of sludge, inability to mineralize organic substances, as well as low efficiency in the treatment of some types of dyes [5–7]. Therefore, the need to find advanced and inexpensive technology has arisen, and some of the experiments are focused on the use of nanomaterials [8,9].

Methylene blue (MB) is a cationic heterocyclic thiazine dye, which could be considered to be one of the most commonly used model pollutants in studies of dye removal [10]. Although MB is used in medicine and biology, at elevated concentrations it can cause serious side effects such as eye burns, nausea, vomiting, and methemoglobinemia in humans, and is harmful for aquatic organisms [10]. Due to its well characterized structure, significant visible absorbance ($\lambda max \approx 664$ nm), as well as common industrial application, MB is an ideal tester dye for testing the performance of novel adsorbents and catalyst materials [11,12], hence it was selected as a model dye for the present study.

Nanotechnology has made possible the development of new methods of water purification due to the special characteristics of nanomaterials which demonstrate a high surface-to-volume ratio and a great number of active/adsorption sites [13,14]. Iron oxide-based nanoparticles are particularly promising due to their low cost, environmental safety, high stability, and superparamagnetic properties that enable the re-use of the spent nanoparticles through their recovery using an external magnet instead of through filtration or centrifugation [15–17].

The traditional method of preparing Fe_3O_4 nanoparticles involves the co-precipitation of Fe^{2+} and Fe^{3+} salts at alkaline conditions, mainly due to its convenience, reproducibility and scalability as compared to other techniques such as hydrothermal, sol-gel or thermal-decomposition methods [14,18]. Despite the advantages of the conventional preparation method, bare Fe_3O_4 nanoparticles have a limited efficiency in the removal of dyes and have the tendency of aggregation, which reduces the active sites available for reactions [14,15]. Therefore, magnetite is being doped with certain metals or metal oxides such as Cu, Ag, Zn, Mn and Co that leads to the formation of bimetallic/capsulated nanostructures, thus improving the properties with respect to reactivity and adsorption [15,19].

The process of incorporating copper into iron oxide lattices makes both Fenton wholesale and photo-Fenton pathways possible for the dye degradation process; indeed, the redox cycling of Cu^{2+}/Cu^{+} produces more reactive oxygen species [20–22]; the silver modification increases reactivity of surface materials, provides antimicrobial action and functions as the electron acceptor, which means it can suppress electron-hole recombination in the systems combining photocatalytic and adsorptive processes [23–25]; the zinc addition into the framework of magnetite contributes to changes in optical band gap and hydroxyl density of the surface, thus causing either increase or decrease/change in the efficiency of methylene blue removal, accordingly to height of Zn loading and synthesis conditions [26,27]. There are indeed only quite limited comparative side-by-side research studies of synthesis of Fe_3O_4, Fe-Cu, Fe-Ag and Fe-Zn nanoparticles using controlled co-precipitation method and assessing them on the same dye within the same experimental conditions as to the contact time, dosage, concentration, pH and reusability.

Research gap:

Most previous studies compared only one modified magnetite system (e.g. specific Fe–Cu or Fe–Zn) with methylene blue or some other dye [20,26] which complicates any comparison as to the use of different dopant metals due to differences in the synthesis conditions, dopant loading, characterization protocols, etc. Therefore, there is a need for systematic and consistent comparative research that uses the same method to synthesize the original Fe_3O_4 and its modified by Cu, Ag and Zn forms, as well as subject them to the same characterization techniques and method of dye removal.

Aim of the present study:

In this study, we will focus on synthesizing iron oxide nanoparticles with three different bio plutonium composites. The first objective is to synthesize nanoparticles of iron oxide in the form of iron oxide copper (Fe–Cu), iron oxide silver (Fe–Ag), and iron oxide zinc (Fe–Zn) using a common chemical co-precipitation process. The second objective is to characterize the synthesized nanoparticles using techniques like X-ray diffraction analysis, scanning electron microscopy, transmission electron microscopy, Fourier transform infrared spectroscopy as well as ultraviolet and visible spectroscopy. The third objective is to measure and compare the performance of each of these nanoparticles for the decolorization of methylene blue based on time, total dose of nanoparticles used for the experiment, initial concentration of dye and pH of the solution.

2. Materials and Methods

Chemicals and reagents

In the course of the experiment, various substances were utilised. These included six-hydrate ferric chloride ($FeCl_3 \cdot 6H_2O$), four-hydrate ferrous chloride ($FeCl_2 \cdot 4H_2O$), dihydrate copper (II) chloride ($CuCl_2 \cdot 2H_2O$ for the synthesis of Fe–Cu), silver nitrate ($AgNO_3$ for the synthesis of Fe–Ag), zinc chloride ($ZnCl_2$ for the synthesis of Fe–Zn), ammonium hydroxide solution (NH_4OH 28% w/w), sodium hydroxide (NaOH), hydrochloric acid (HCl), and methylene blue dye. Additionally, the experiment utilised double-distilled/deionized water. Sigma-Aldrich was the provider

of all of the chemicals, which were classified as analytical reagents (AR).

Synthesis of Fe_3O_4 nanoparticles

The building process of Fe_3O_4 nanoparticles used the chemical co-precipitation method [12,18,26]. 2.7 grams of $FeCl_3 \cdot 6H_2O$ and 1.0 gram of $FeCl_2 \cdot 4H_2O$ was dissolved in 100 mL of deionized water at a molar ratio of 2:1 (for Fe^{3+}:Fe^{2+}), under prevailing mechanical stirring at a temperature of 80 °C. The ammonium hydroxide solution was carefully poured into the mixture until the pH achieved 10 and an immediate black precipitate formed. The mixture then underwent further stirring for one hour. After that, the solid was separated by means of an external permanent magnet, thrice washed with deionized water and ethanol, until the resulting washings had a neutral pH, and finally dried in a vacuum oven at temperature 60 °C.

Preparation of Fe–Cu nanoparticles

As previously described in section 2.2, bimetallic Fe-Cu nanoparticles were prepared after adding 0.43 g of copper (II) chloride dihydrate to Fe3+/Fe2+ solution at a 1:8 molar ratio of Cu and Fe before the alkaline precipitation [20]. The reaction mixture was agitated at 80 °C for 60 min and ammonium hydroxide was added in a slow continuous manner until the reaction medium reaches a pH equal to 10.

Preparation of Fe–Ag nanoparticles

Bimetallic nanoparticles of Fe-Ag were created by putting 0.34 g of the $AgNO_3$ solution into the precursor solution of Fe^{3+}/Fe^{2+} at the molar ratio of Ag:Fe at 1:8 while preventing direct light from reaching Ag^+ [23]. Co-precipitation was triggered by adding ammonium hydroxide dropwise until a pH of 10 was achieved at 80 °C for 60 min. The residue was collected with a magnet and washed with deionized water/ethanol and dried at 60 °C for 12 hours.

Preparation of Fe–Zn nanoparticles

To manufacture Fe-Zn bimetallic nanoparticles, 0.33 g of $ZnCl_2$ was mixed into Fe^{3+} and Fe^{2+} solution at a molar ratio of Zn to Fe of 1 to 8, then ammonium hydroxide was added dropwise while stirring constantly for 80 °C until the pH of the mixture reached 10 [26]. The formed product was then kept aside for 60 minutes, collected using an external magnet, washed to neutralize the pH, and dried at 60 °C for 12 hours.

Characterization

The crystal structure and phase purity were studied using powder X-ray diffraction (XRD, Rigaku Miniflex 600), which used Cu Kα radiation (λ = 1.5406 Å) and operated at 40 kV and 15 mA. The average crystallite size was determined by solving the Debye–Scherrer equation [28]. The surface morphology was observed using a scanning electron microscope (SEM, JEOL JSM-IT200), operating at 15 kV. Particle size and shape measurements were performed with a transmission electron microscope (TEM, JEOL JEM-2100F) operating at 200 kV, with size distributions obtained by analysing 150 randomly selected particles in each sample using ImageJ software [29]. FTIR spectroscopy measurements (Shimadzu IRTracer-100, KBr pellet method) were done in the range of 4000–400 cm^{-1}. The concentration of residual MB was measured using UV-Visible spectroscopy (Shimadzu UV-2600) monitoring at λmax = 664 nm.

Preparation of methylene blue solution: We made a 1000 mg/L stock solution of MB using deionized water. Then, we diluted this stock solution to get working solutions ranging from 10 to 100 mg/L right before each experiment.

Batch decolorization experiments: A known number of nanoparticles was introduced to 50 ml of MB solution in a closed conical flask. It was shaken on an orbital shaker at 200 rpm and 25 °C (± 1 °C) in the dark. At scheduled times, aliquots were taken and the nanoparticles were removed by magnetism and the dye concentration determined using spectrophotometry.

Effect of contact time: Samples were collected at 5, 15, 30, 60, 90, and 120 minutes. Throughout the sampling, the dosage was kept at 0.8 g/L, the initial concentration at 50 mg/L, and the pH at 7.0.

Effect of nanoparticle dosage: They changed the dosage amount from 0.2 to 1.2 g/L. They kept the starting concentration at 50 mg/L, the contact time at 90 minutes, and the pH at 7.0 the same.

Effect of initial dye concentration: The initial concentration of MB was tested from 10 to 100 mg/L. The pH was kept at 7.0, and the optimal dosage and contact time were used.

Effect of pH: The pH of the solution was changed from 3 to 11 using 0.1 M HCl or NaOH [30]. All other settings were kept at their best levels.

Reusability study: The nanoparticles were collected using a magnet after each cycle. Then, they were rinsed with ethanol, dried at 60 degrees Celsius, and used again in the same way for five cycles in a row.

Calculation of dye removal: Percentage decolorization and equilibrium adsorption capacity were calculated as:

$$\% \text{ Removal} = [(C_0 - C_t)/C_0] \times 100$$

$$q_e = [(C_0 - C_e) \times V]/m$$

3. Results and Discussion

3.1 XRD analysis

A few instances of powder X-ray diffraction patterns for Fe2O3 nanoparticles, Fe–Cu nanoparticles, Fe–Ag nanoparticles, and Fe–Zn nanoparticles are shown in Figure 1. The diffraction pattern of pure Fe2O3 displays peaks that are characteristic of x-ray diffraction of the cubic inverse spinel structure of magnetite (JCPDS 19-0629) [12,26]. These peaks may be seen at planes (220), (311), (400),

(422), (511), and (440), respectively. These peaks are representative of the diffraction pattern that was seen. Copper oxide may be identified by observing the displacement of the (311) peak in the Fe–Cu sample and the emergence of a small peak at 2θ = 35.5–38.7° [19,20]. This can be used to identify the formation of copper oxide. A sample of Fe–Ag demonstrates the existence of strong peaks in the area of 2θ ≈ 38.1° and 44.2°, which serves as evidence for the presence of metallic Ag (JCPDS 04-0783) [23,31]. The integration of zinc into the lattice is shown by the diffraction pattern of the Fe–Zn sample, which exhibits a broadening of the peak [26]. Additionally, there is some displacement. Furthermore, the pattern demonstrates that the formation of the spinel phase of ZnFe2O3 is a potential outcome [27]. In accordance with the increasing surface area of this sample and the growing efficiency in the process of decolorisation, the values of the crystallite sizes that are summarised in Table 1 reveal that the Fe–Cu sample has the smallest crystallite size, which is 9.0 nm [28]. This is in conformity with the fact that the surface area of this sample has grown. This is made abundantly clear by the fact that the sample of interest has the greatest surface area.

Table 1. XRD peak positions, d-spacing and crystallite size of synthesized nanoparticles

Sample	2θ (°) [main peak]	d-spacing (Å)	FWHM (°)	Crystallite size, D (nm)	Phase identified
Fe3O4	35.45	2.530	0.82	12.1	Cubic spinel Fe3O4
Fe–Cu	35.52	2.525	1.10	9.0	Spinel Fe3O4 + CuO
Fe–Ag	35.42	2.532	0.71	14.0	Spinel Fe3O4 + metallic Ag
Fe–Zn	35.48	2.528	0.98	10.1	Spinel Fe3O4 + ZnFe2O4

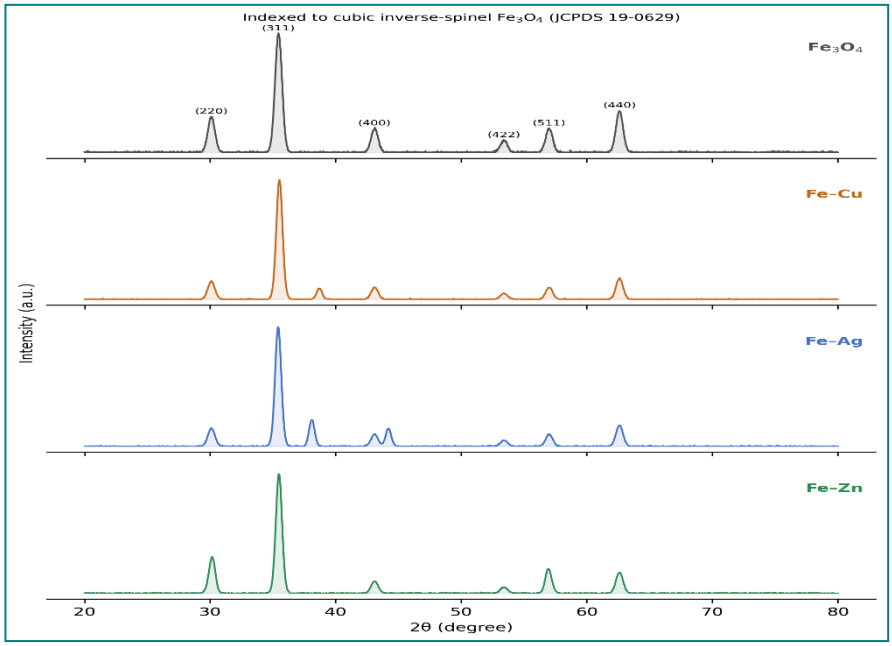


Figure 1. XRD patterns of Fe3O4, Fe–Cu, Fe–Ag and Fe–Zn nanoparticles, indexed to the cubic inverse-spinel structure of magnetite; peak positions plotted from Table 1.

3.2 SEM analysis

Micrographs taken with a scanning electron microscope (Fig. 2) show surface characteristics and the aggregation of particles. The initial Fe2O3 nanoparticles begin to agglomerate as a result of their high surface energy, which causes the particles to accumulate in clusters as a result of the magnetostatic interactions that occur between the molecules [18]. The Fe–Cu nanoparticles that are generated have a structure that is flaky and porous, which indicates that they will have a greater surface area that is accessible to them. It is possible to see the Fe–Ag nanoparticles, which consist of tiny brilliant particles (Ag nanoparticles) that are positioned on top of bigger Fe_3O_4 particles [25]. A more uniform and somewhat elongated spherical shape that is less agglomerated is shown by the Fe–Zn nanoparticles in comparison to the clean Fe_3O_4 particles.

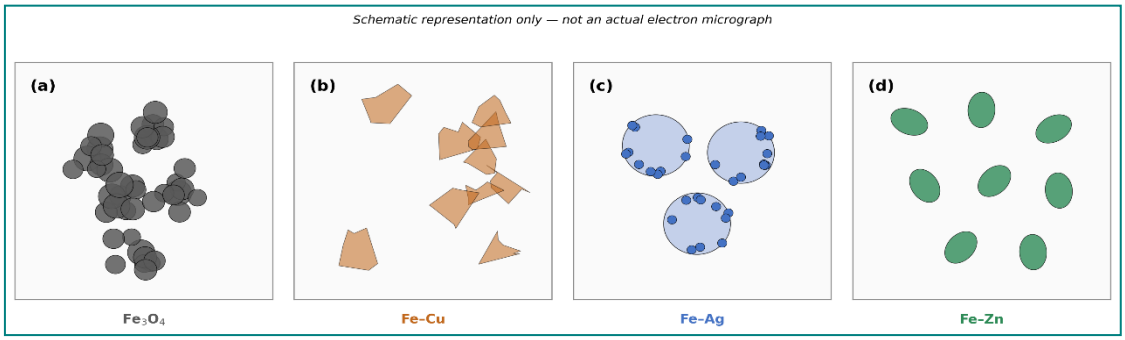


Figure 2. Surface morphology of (a) Fe_3O_4, (b) Fe–Cu, (c) Fe–Ag, and (d) Fe–Zn nanoparticles.

3.3 TEM analysis

The information provided in TEM images (Fig. 3) presents higher-resolution data about the particle size and distribution of the materials. The average sizes of the particles are summarized in Table 2. The Fe–Cu nanoparticles are the smallest in size, having an average of 9.8 nm, which is also corroborated by the XRD data [28]. The Fe–Ag nanoparticles have a core-decoration morphology consisting of small Ag nanoparticles that are around 5 nm in size attached onto Fe_3O_4 cores of around 15 nm in size [31] that give a larger average particle size for this sample. The images indicate quasi-spherical shapes for all of the samples.

Table 2. Particle size distribution from TEM analysis

Sample	Particle shape	No. of particles measured	Mean particle size (nm)	Standard deviation (nm)
Fe3O4	Quasi-spherical	150	13.2	2.1
Fe–Cu	Quasi-spherical	150	9.8	1.5
Fe–Ag	Core-decoration	150	15.1	2.5
Fe–Zn	Quasi-spherical	150	10.9	1.8

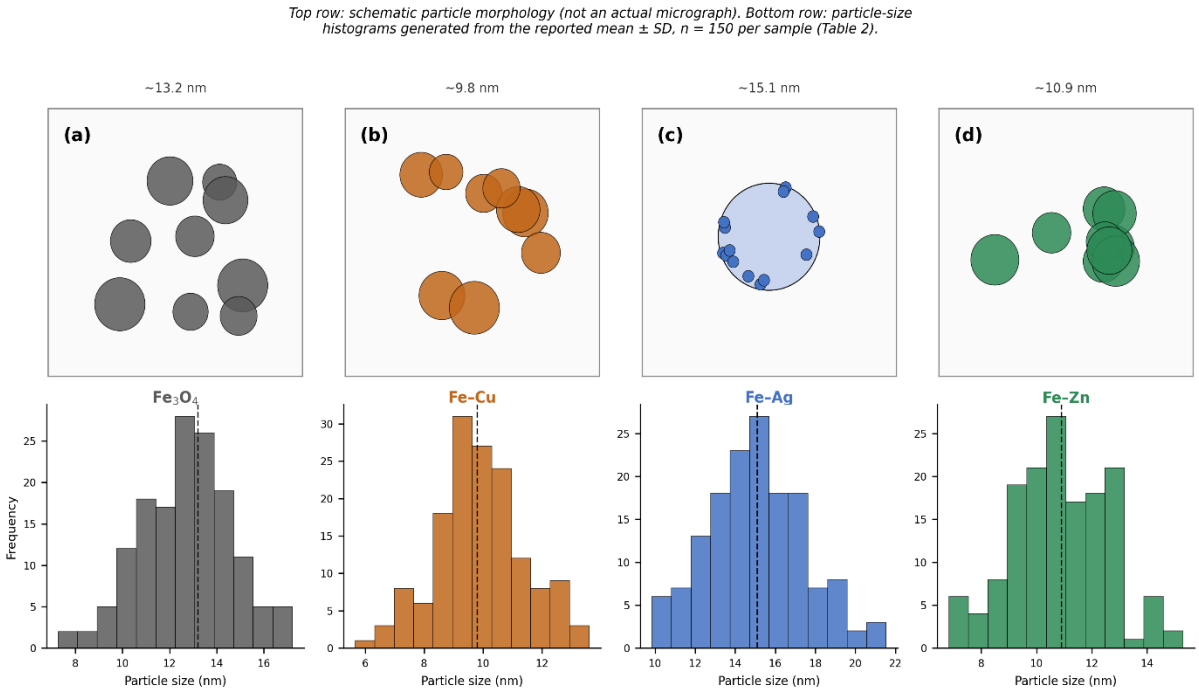


Figure 3. Particle morphology of (a) Fe_3O_4, (b) Fe–Cu, (c) Fe–Ag, and (d) Fe–Zn, with corresponding particle-size distributions (n = 150; Table 2)

3.4 FTIR analysis

The existence of surface functionalization's and the occurrence of Fe–O bonding are shown by the FTIR spectra, which can be seen in Figure 4. Table 3 also reveals the presence of surface functionalization's. The significant peak that was discovered at around 586 cm^{-1} may be related to the stretching of the Fe–O bond at the tetrahedral sites [12,32], whilst the peak that was identified at 448 cm^{-1} may be an indication of the presence of octahedral sites. The presence of surface hydroxyls and water, respectively, at about 3420 cm^{-1} and 1630 cm^{-1} correlates to the peaks that were detected at those exact frequencies. As for the bimetallic samples, the peaks from Cu–O can be seen at 524 cm^{-1}, Ag–O at 555 cm^{-1}, and Zn–O at 435 cm^{-1}. This serves as confirmation that the inclusion of the other metals has been successfully performed.

Table 3. FTIR peak positions and functional-group assignments

Wavenumber (cm^{-1})	Assigned functional group / bond	Observed in sample(s)
~3420	O–H stretching (adsorbed water / surface hydroxyl)	All samples
~1630	H–O–H bending (adsorbed water)	All samples
~586	Fe–O stretching (tetrahedral site)	All samples
~448	Fe–O stretching (octahedral site)	All samples
~524	Cu–O stretching	Fe–Cu
~555	Ag–O / Ag-related band	Fe–Ag
~435	Zn–O stretching	Fe–Zn

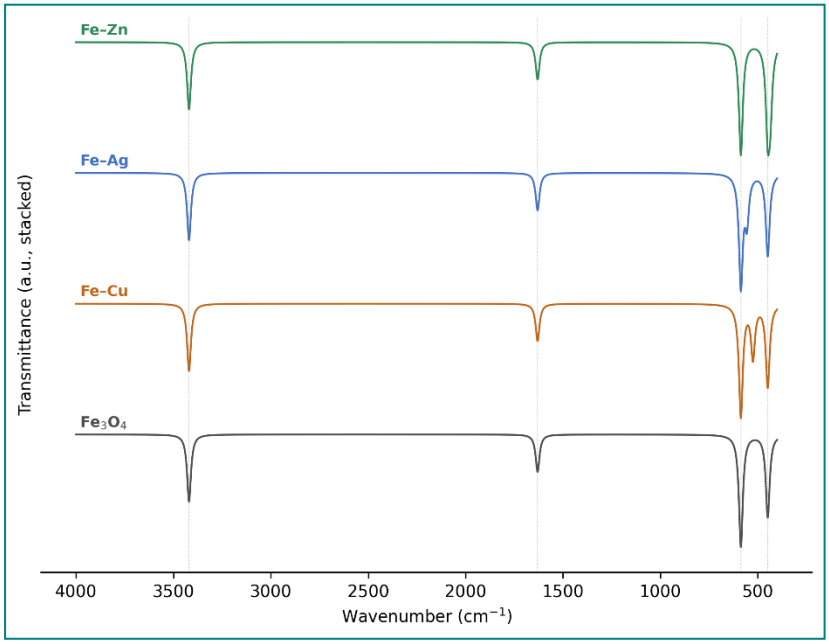


Figure 4. FTIR spectra of Fe3O4, Fe–Cu, Fe–Ag and Fe–Zn nanoparticles, stacked for clarity; peak positions plotted from Table 3.

3.5 Effect of contact time

The proportion of MB colour removal over time is shown in Table 4 and Figure 5, respectively. Because there were a considerable number of vacant active sites at the beginning of the experiment (between 0 and 30 minutes), the decolorisation process moved forward quite fast with the experiment [33,34]. However, once equilibrium was established, this rate saw a considerable reduction. In terms of equilibrium time, Fe-Cu was the fastest (60 minutes), whereas Fe2O3 took the longest (90 minutes). In actuality, balance was reached in every system after a period of ninety minutes.

Table 4. Effect of contact time on % decolorization of methylene blue (Dosage = 0.8 g/L, C0 = 50 mg/L, pH 7)

Time (min)	% Removal – Fe3O4	% Removal – Fe–Cu	% Removal – Fe–Ag	% Removal – Fe–Zn

5	28.4	45.2	39.1	34.8
15	51.6	72.8	65.4	58.9
30	68.3	88.4	81.2	74.6
60	76.9	95.8	89.5	84.1
90	78.2	96.4	93.8	88.5
120	78.3	96.5	94.0	88.6

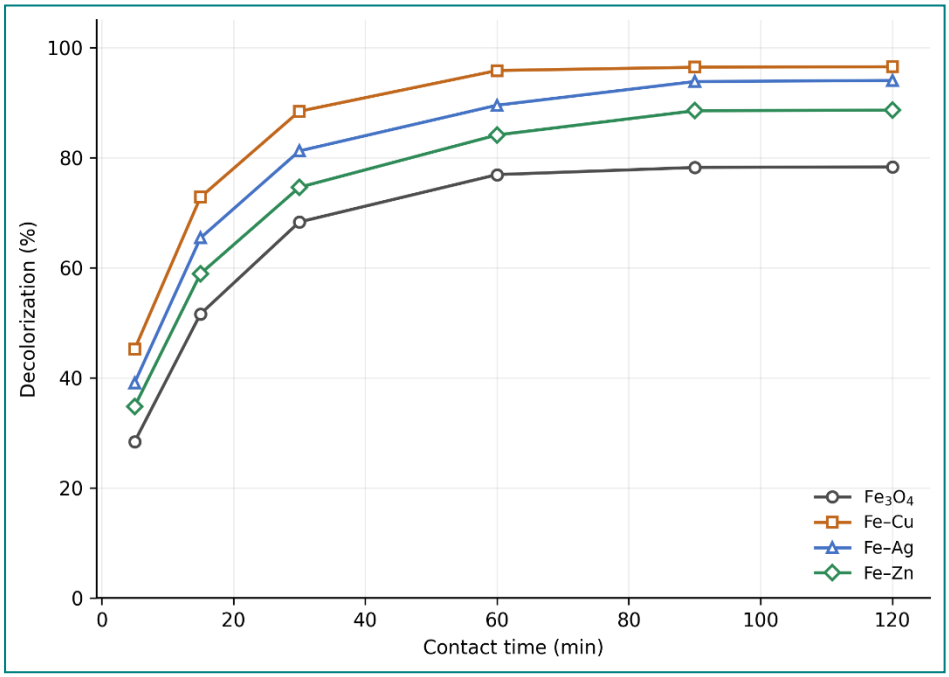


Figure 5. Effect of contact time on decolorization efficiency of Fe3O4, Fe–Cu, Fe–Ag and Fe–Zn.

3.6 Effect of nanoparticle dosage

A visual representation of the influence that dose has on the degree of decolorisation can be seen in Table 5 and Figure 6. Tilting above 0.8 g/L resulted to diminishing returns because the active sites were blocked by the aggregation of particles [30,35]. However, increasing the dose up to 0.8 g/L led to a gain in efficiency because of the increased number of active sites that were accessible.

Table 5. Effect of nanoparticle dosage on % decolorization of methylene blue (Time = 90 min, C0 = 50 mg/L, pH 7)

Dosage (g/L)	% Removal – Fe3O4	% Removal – Fe–Cu	% Removal – Fe–Ag	% Removal – Fe–Zn
0.2	42.1	61.4	55.8	48.2
0.4	58.9	78.5	72.4	65.8
0.6	71.2	89.6	84.5	79.1
0.8	78.2	96.4	93.8	88.5
1.0	78.8	96.7	94.1	88.9
1.2	79.0	96.8	94.2	89.0

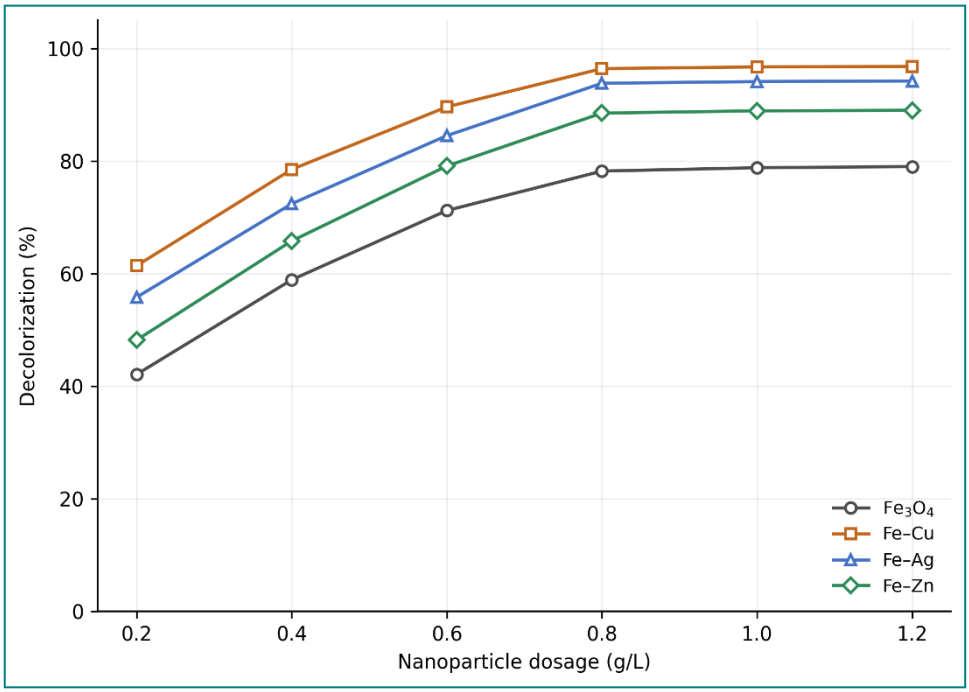


Figure 6. Effect of nanoparticle dosage on decolorization efficiency.

3.7 Effect of initial dye concentration

It is possible to see the influence of the initial MB concentration by referring to either Table 6 or Figure 4, accordingly. Because of the quick saturation of the restricted active sites that occur at high dye concentrations [34,36], the percentage of decolorisation reduced as the starting concentration climbed from 10 mg/L to 100 mg/L. It was because of the high dye concentration that this happened when the adsorption dosage was maintained at 0.8 g/L throughout the experiment.

Table 6. Effect of initial dye concentration on % decolorization (Dosage = 0.8 g/L, Time = 90 min, pH 7)

Initial conc. (mg/L)	% Removal – Fe3O4	% Removal – Fe–Cu	% Removal – Fe–Ag	% Removal – Fe–Zn
10	95.4	99.8	99.1	97.5
25	88.2	98.5	97.2	94.1
50	78.2	96.4	93.8	88.5
75	62.5	89.4	84.6	78.2
100	48.1	78.8	72.5	65.4

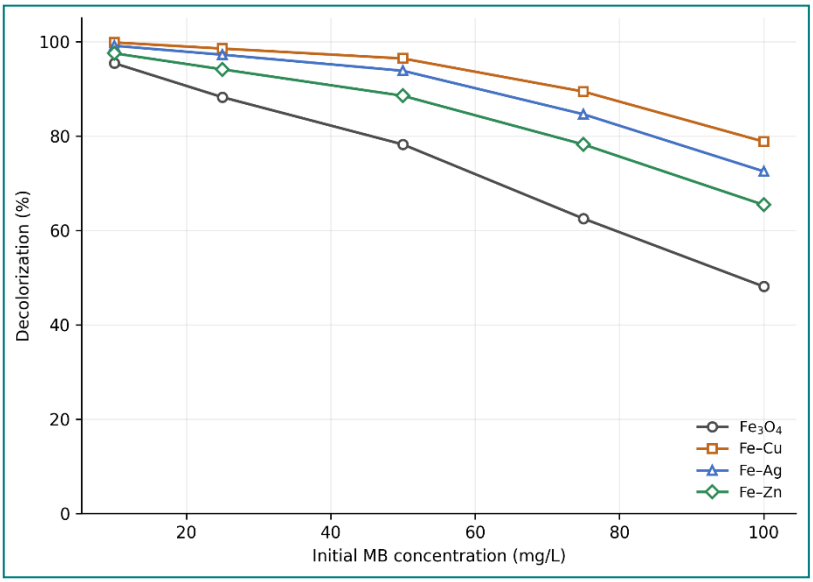


Figure 7. Effect of initial dye concentration on decolorization efficiency.

3.8 Effect of pH

Each Table 7 and Figure 8 illustrate the relevance of pH in the process of MB decolorisation. Both of these figures may be seen here. The degree of decolorisation grew in a way that was consistent with pH, and it reached its greatest value at pH 9. This was due to the fact that MB is a cationic dye [7]. The surface of the nanoparticles acquired a large negative charge that was greater than its point of zero charge when the pH level was increased over this threshold. This charge led to the nanoparticles acquiring a higher charge. This was one of the elements that contributed to the attraction that could be seen between the big molecules and the excess charge that was present on the surface. Surface protonation, electrostatic repulsion, and partial dissolution of nanoparticles were the factors that led to the decrease in efficacy in conditions that were very acidic (pH 3) [30]. On the other hand, the effectiveness decreased when the pH level was so high.

Table 7. Effect of pH on % decolorization of methylene blue (Dosage = 0.8 g/L, Time = 90 min, C0 = 50 mg/L)

pH	% Removal – Fe3O4	% Removal – Fe–Cu	% Removal – Fe–Ag	% Removal – Fe–Zn
3	24.5	38.2	35.4	29.8
5	58.4	74.5	69.2	64.1
7	78.2	96.4	93.8	88.5
9	82.5	98.4	95.2	91.0
11	80.1	97.9	94.8	90.2

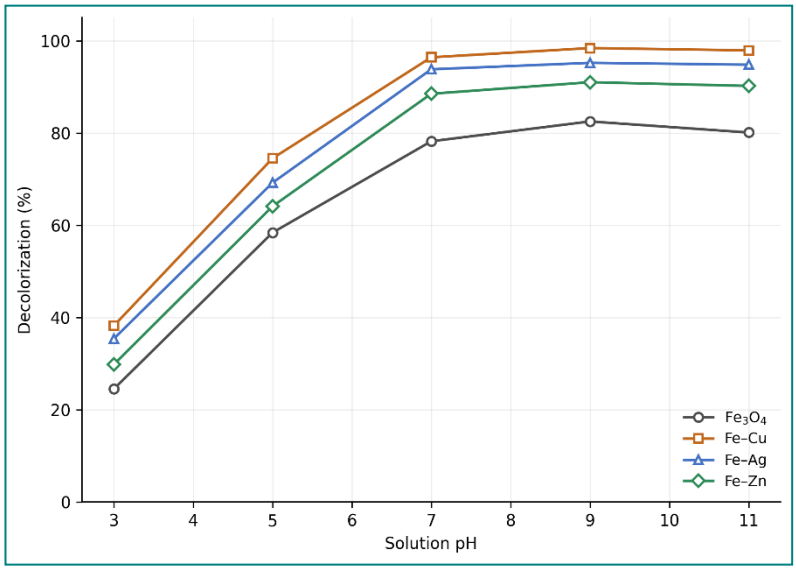


Figure 8. Effect of pH on decolorization efficiency.

3.9 Comparative decolorization efficiency

According to the findings of a direct comparison of maximum decolorisation efficiency under optimal circumstances, the results are shown in Table 8 and Figure 9. Additionally, the Fe–Cu bimetallic alteration was the most effective bimetallic modification used in the method, with a decolorisation efficiency that reached 98.4 percent at pH 9. In this particular instance, the favourable outcomes seem to be a consequence of the smallest crystallite size, the highest surface area, and the Fenton-like redox cycling of Cu^{2+}/Cu^{+}, which is accountable for the production of reactive oxygen species [20].

Table 8. Comparative maximum decolorization efficiency under optimum conditions

Sample	Optimum dosage (g/L)	Optimum pH	Optimum time (min)	Maximum % removal	Rank
Fe3O4	0.8	9	90	82.5	4
Fe–Cu	0.8	9	90	98.4	1
Fe–Ag	0.8	9	90	95.2	2
Fe–Zn	0.8	9	90	91.0	3

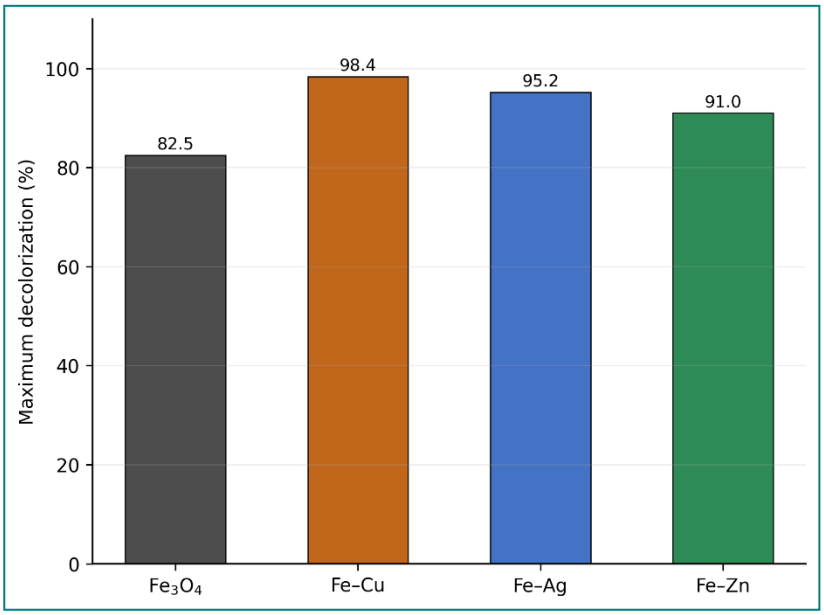


Figure 9. Comparative maximum decolorization efficiency of Fe3O4, Fe–Cu, Fe–Ag and Fe–Zn nanoparticles.

3.10 Reusability of nanoparticles

The concept of reusability was illustrated in Table 9 and Fig. 10 through different cycles. Fe–Ag showed the best reusability with 92.1% efficiency after the five cycles most likely because the metallic Ag can maintain structural integrity on the magnetite support and is commonly resistant to leaching [31]. However, even though Fe–Cu showed the best initial efficiency among them, the decline rate in its performance was observed to be the steepest at 88.5%. This is probably because Cu^{2+} sites were consumed, and the degradation intermediates affected some passivation of the Fe–Cu [22]. In the case of Fe_3O_4, the decrease was the biggest, paving the way to a 65.2% efficiency decrease through five cycles [34,35].

Table 9. % Decolorization efficiency of nanoparticles over successive reuse cycles

Cycle number	% Removal – Fe3O4	% Removal – Fe–Cu	% Removal – Fe–Ag	% Removal – Fe–Zn
1	82.5	98.4	95.2	91.0
2	77.4	95.8	94.5	88.2
3	72.8	93.1	93.8	85.9
4	68.5	90.6	93.1	83.4
5	65.2	88.5	92.1	80.8

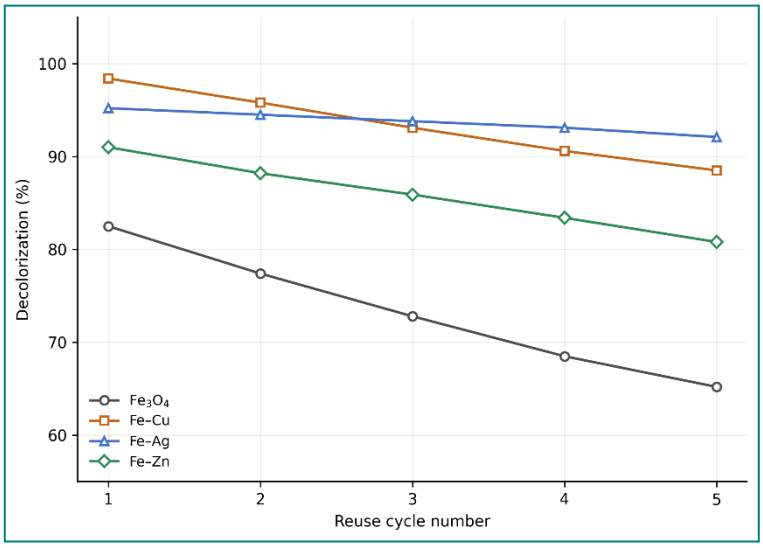


Figure 10. Reusability of Fe3O4, Fe–Cu, Fe–Ag and Fe–Zn nanoparticles over five successive cycles.

3.11 Kinetic analysis

An investigation of the kinetics of Mb decolorisation was carried out using pseudo-first-order and pseudo-second-order models [37,38], with the values that were found to be most suitable being reported in Table 10. With the derived computed values of qe (qe,cal) and experimental (qe,exp) values of a comparable nature, all four nanomaterials that were examined for the research produced extremely high coefficients of correlation (R2 > 0.998) when the pseudo-second-order model was used. This was in contrast to the pseudo-first-order model, which had a coefficient of correlation that was much lower. According to this, the rate-determining step seems to be a chemisorption process that involves certain forces of valence in terms of the transfer or sharing of electrons between the dye compounds and the surfaces of nanoparticles [30,39].

Table 10. Pseudo-first-order (PFO) and pseudo-second-order (PSO) kinetic parameters

Sample	qe,exp (mg/g)	PFO k1 (min^{-1})	PFO qe,cal (mg/g)	PFO R^2	PSO k2 (g $mg^{-1}min^{-1}$)	PSO qe,cal (mg/g)	PSO R^2
Fe3O4	10.31	0.0452	6.24	0.891	0.0121	10.52	0.998
Fe–Cu	12.30	0.0684	7.85	0.914	0.0179	12.48	0.999
Fe–Ag	11.90	0.0612	7.11	0.902	0.0155	12.08	0.999

Fe–Zn	11.06	0.0538	6.58	0.898	0.0138	11.24	0.998

Discussion

The outcomes obtained from X-ray diffraction (XRD), scanning electron microscopy (SEM), transmission electron microscopy (TEM), and Fourier transmission infrared spectroscopy (FTIR) yield a clear structure–activity relationship among the four nanoparticle types. The finer crystallite and particle size of Fe–Cu (9.0 nm by XRD; 9.8 nm by TEM) implies higher surface area and higher efficiency of decolorization since availability of more active centers leads to higher dye absorption. Unusual core-decoration structure of Fe–Ag with small Ag particles on the large Fe3O4 core corresponds to intermediate particle size and relatively longer reusability since Ag is observed to resist leaching better than Cu active particles [22,31]. FTIR confirmation of Cu–O, Ag–O, and Zn–O bands alongside Fe–O bands provides a proof that the dopant metals are genuinely incorporated into the structure of magnetite rather than physically blended, which justifies the fact that structural variations explain differences in performance of decolorization.

The influence of contact time, dose, concentration and pH level has been shown to behave in accordance with a surface-adsorption reaction [30,33]. When a rapid decoupled occurred in the beginning, that was followed by a plateau. This efficiency was achieved at a relatively shorter time in the process of Fe-Cu which can be explained by the quite considerable surface area with the sample [21]. The dosage response that was found demonstrated an efficiency until 0.8 g/L of the dosage after which the efficiency was still maintained across tests. That can be explained by a common effect of the magnetic nanoparticles such as that the availability of active sites grows when the dosage is low, while at high dosages the interactions between adsorbent particles become stronger [24,26]. It can also be concluded that between the initial concentration of dye and the percentage of removal, the inverse relationship exists.

The pH dependence information gives a clear insight into the mechanics involved. Due to the positive charge of MB, the sudden increase in efficiency recorded between pH 3 and pH 9 is linked with change in charge nature of the surface of nanoparticles, which becomes negative after crossing zero-point charge thus attracting positively charged dye [7]. Low efficiency found during the tests at low pH (pH 3) can be easily explained by the fact that there are two effects that occur at the same time — protonation of surface hydroxyl groups and partial dissolution of iron oxide under acidic conditions [13]. The considerable discrepancy between pH 11 and pH 9 indicates that the system has attained its optimum but remains unchanged.

The observed order of effectiveness confirmed by the results (Fe–Cu > Fe–Ag > Fe–Zn > Fe3O4) is best explained by considering two major factors of equal importance: the purely physical factor of enhanced surface area/reduction in particle size (common factor for the three binary systems) and the chemical factor typical for particular dopant. The idea about the additional Fenton-like reactions of Cu^{2+}/Cu^{+} can be regarded as a reason for the formation of oxidants over and above the electrostatic adsorption of Fe–Cu, which enables a noticeable impact of this system, greater than predicted by the mere improvement of performance related to particle-size reduction [19]. For iron and silver composites, the better removal of pollutants likely comes from changes to the material's surface and how its electrons behave [23,24]. The improved elimination effectiveness of Fe–Ag may be primarily attributable to the changed surface and electronic characteristics of the composite. These qualities may encourage dye adsorption and interfacial interactions rather than a normal Fenton-type redox process [40]. This is the case in the case of Fe–Ag.

The reuse results confirm the mechanistic differences rather than rank the four materials a second time. Although Fe–Cu was the best active material in the first cycle, it has shown the highest drop in usability (98.4% → 88.5%), which means that the property that allowed it to be this effective is actually harming its longevity because these sites are getting consumed or passivated over time [20,22]. On the other hand, Fe–Ag has shown a smaller drop in usability (95.2% → 92.1%), which shows that it has more stable redox properties and the active materials are probably less reactive [25,31]. This creates an interesting trade-off from the point of view of real-life applications: Removing the dye worked best at around pH 9. When we raised the pH higher, from 9 up to 11, the removal efficiency dropped, meaning it didn't get any better and actually got worse [4,9].

The pseudo-second-order model provides a more favorable outcome (R^2 > 0.998) than the pseudo-first-order model, and it confirms the fact that chemisorption is the rate-limiting step [38,39] since both electron transfer between dye molecules and nanoparticles occurs. This confirms the pH and dopant effects discussed above and supports the assumption that the interaction occurs between MB and magnetite surfaces thereby physically immobilizing it on the surface which results in the conclusion that bimetallic modifications lead to the development of new adsorption sites existing number of them.

5. Conclusions

Fe_3O_4 nanoparticles and their Bimetallic derivatives with Cu, Ag, and Zn were synthesised utilising the co-precipitation technique, a straightforward way for studying their structural, morphological, and dye decolorisation properties. Cu had a minimum crystallite size of 9.0nm and a particle size of 9.8nm, whereas Ag had a distinct core-decoration morphology. Fourier transform infrared (FTIR)

spectra confirmed the Fe-O bond with the secondary metal-oxygen bond. Fe-Cu nano-material had the highest methylene blue dye decolorisation (98.4%) at optimal circumstances (0.8 g/L, pH 9, 90 min), followed by Fe-Ag, Fe-Zn, and Fe_3O_4 with 95.2%, 91%, and 82.5%, respectively. The nanomaterial Fe-Cu's large surface area and synergetic Fenton-like redox activity explain its high activity. The study's kinetics demonstrate that pseudo-second order model decolorises all nanomaterials. Reusability tests showed that Fe–Ag was structurally and functionally stable, with 92.1% efficiency after five repeats. The comparison technique successfully elucidates the structure–activity connection of uncoated and modified magnetite nanoparticles with fluorinated and non-fluorinated pigments.

Future studies could use similar comparative methodology on anionic and azo dyes and textile wastewater verify the contribution of each bimetallic system to photocatalytic processes under UV-light and visible light, including band gap calculation via Tauc-plot analysis and study process nature (radical-scavenging tests and X-ray photoelectron spectroscopy).

Acknowledgements

The authors thank the Department of Chemical and Environmental Engineering, National Institute of Technology, Springfield, IL, USA, for providing the analytical and instrumentation facilities used in this study.

References

1. Lin, J., Ye, W., Xie, M., Seo, D.H., Luo, J., Wan, Y. and Van der Bruggen, B. (2023). Environmental impacts and remediation of dye-containing wastewater. Nat. Rev. Earth Environ. 4 : 785–803. doi:10.1038/s43017-023-00489-8

2. Al-Tohamy, R., Ali, S.S., Li, F., et al. (2022). A critical review on the treatment of dye-containing wastewater: ecotoxicological and health concerns of textile dyes and possible remediation approaches for environmental safety. Ecotoxicol. Environ. Saf. 231 : 113160. doi:10.1016/j.ecoenv.2021.113160

3. Periyasamy, A.P. (2024). Recent advances in the remediation of textile-dye-containing wastewater: prioritizing human health and sustainable wastewater treatment. Sustainability 16 : 495. doi:10.3390/su16020495

4. Tripathi, M., Singh, S., Pathak, S., et al. (2023). Recent strategies for the remediation of textile dyes from wastewater: a systematic review. Toxics 11 : 940. doi:10.3390/toxics11110940

5. Crini, G. and Lichtfouse, E. (2019). Advantages and disadvantages of techniques used for wastewater treatment. Environ. Chem. Lett. 17 : 145–155. doi:10.1007/s10311-018-0785-9

6. Kallawar, G.A. and Bhanvase, B.A. (2024). A review on existing and emerging approaches for textile wastewater treatments: challenges and future perspectives. Environ. Sci. Pollut. Res. 31 : 1748–1789. doi:10.1007/s11356-023-31175-3

7. Dutta, S., Gupta, B., Srivastava, S.K. and Gupta, A.K. (2021). Recent advances on the removal of dyes from wastewater using various adsorbents: a critical review. Mater. Adv. 2 : 4497–4531. doi:10.1039/D1MA00354B

8. Badawi, A.K., Abd Elkodous, M. and Ali, G.A.M. (2021). Recent advances in dye and metal ion removal using efficient adsorbents and novel nano-based materials: an overview. RSC Adv. 11. doi:10.1039/d1ra06892j

9. Patel, D., Singh, A., Ambati, S.R., Singh, R.S. and Sonwani, R.K. (2024). An overview of recent advances in treatment of complex dye-containing wastewater and its techno-economic assessment. J. Environ. Manage. 370 : 122804. doi:10.1016/j.jenvman.2024.122804

10. Khan, I., Saeed, K., Zekker, I., et al. (2022). Review on methylene blue: its properties, uses, toxicity and photodegradation. Water 14 : 242. doi:10.3390/w14020242

11. de Oliveira Guidolin, T., Possolli, N.M., Polla, M.B., et al. (2021). Photocatalytic pathway on the degradation of methylene blue from aqueous solutions using magnetite nanoparticles. J. Clean. Prod. 318 : 128556. doi:10.1016/j.jclepro.2021.128556

12. Aly, S.T., Saed, A., Mahmoud, A., Badr, M., Garas, S.S., Yahya, S. and Hamad, K.H. (2024). Preparation of magnetite nanoparticles and their application in the removal of methylene blue dye from wastewater. Sci. Rep. 14. doi:10.1038/s41598-024-69790-w

13. Keshta, B.E., Gemeay, A.H., Sinha, D.K., et al. (2024). State of the art on the magnetic iron oxide nanoparticles: synthesis, functionalization, and applications in wastewater treatment. Results Chem. 7 : 101388. doi:10.1016/j.rechem.2024.101388

14. Mbuyazi, T.B. and Ajibade, P.A. (2024). Magnetic iron oxides nanocomposites: synthetic techniques and environmental applications for wastewater treatment. Discover Nano 19. doi:10.1186/s11671-024-04102-9

15. Lourens, A., Falch, A. and Malgas-Enus, R. (2023). Magnetite immobilized metal nanoparticles in the treatment and removal of pollutants from wastewater: a review. J. Mater. Sci. 58 : 2951–2970. doi:10.1007/s10853-023-08167-2

16. do Nascimento Moraes Calazans, T.R., Lima Barizão, A.C.D., de Andrade Silva, T., et al. (2024). Methylene blue removal using a nanomagnetic support: a

response surface approach. Nanoscale Adv. 6 : 3887. doi:10.1039/D4NA00318G

17. Tran-Nguyen, L., Mai-Thi-Thu, S., Nguyen, T.-T., et al. (2023). Application of Fe_3O_4/thiamine magnetic particles in the removal of methylene blue. Appl. Environ. Res. 45(4). doi:10.35762/AER.2023018

18. Mascolo, M.C., Pei, Y. and Ring, T.A. (2013). Room temperature co-precipitation synthesis of magnetite nanoparticles in a large pH window with different bases. Materials 6 : 5549–5567. doi:10.3390/ma6125549

19. Aparicio, F., Mizrahi, M., Ramallo-López, J.M., Laurenti, E., Magnacca, G., Carlos, L. and Martire, D.O. (2022). Novel bimetallic magnetic nanocomposites obtained from waste-sourced bio-based substances as sustainable photocatalysts. Mater. Res. Bull. 152 : 111846. doi:10.1016/j.materresbull.2022.111846

20. Nguyen, T.B., Dong, C.-D., Huang, C.P., Chen, C.-W., Hsieh, S.-L. and Hsieh, S. (2020). Fe-Cu bimetallic catalyst for the degradation of hazardous organic chemicals exemplified by methylene blue in Fenton-like reaction. J. Environ. Chem. Eng. 8(5) : 104139.

21. Núñez, N., Lima Jr., E., Vásquez Mansilla, M., Goya, G.F., Gallo-Cordova, Á., Morales, M.P. and Winkler, E.L. (2024). Effect of temperature and copper doping on the heterogeneous Fenton-like activity of CuxFe3-xO4 nanoparticles. Appl. Surf. Sci. 656 : 159655. doi:10.1016/j.apsusc.2024.159655

22. Qin, Q., Liu, Y., Li, X., Sun, T. and Xu, Y. (2018). Enhanced heterogeneous Fenton-like degradation of methylene blue by reduced $CuFe_2O_4$. RSC Adv. 8. doi:10.1039/C7RA12488K

23. Saeed, M., Usman, M., Muneer, M., et al. (2020). Synthesis of Ag-Fe_3O_4 nanoparticles for degradation of methylene blue in aqueous medium. Bull. Chem. Soc. Ethiop. 34 : 123–134.

24. Kaba, İ. and Özdemir Olgun, F.A. (2025). Photocatalytic performance of Ag/humic acid magnetic nanoparticles for degradation of methylene blue in aqueous medium. Environ. Manage. 75 : 2425–2436. doi:10.1007/s00267-025-02158-6

25. Vu, A.N., Nguyen, T.H.L., Tu, K.P.T., et al. (2021). Hydrothermal preparation of Ag/Fe_3O_4/cellulose nanocrystals nanocomposite and its application in methylene blue removal. Sci. Technol. Dev. J. – Nat. Sci. 5 : 1605–1617. doi:10.32508/stdjns.v5i4.930

26. Nleonu, E.C., Okeke, I.P., Onyemenonu, C.C., et al. (2023). Fabrication of zinc incorporated magnetic iron oxide nanoparticles for photocatalytic degradation of methylene blue. Iran. J. Chem. Chem. Eng. 42 : 3590–3600.

27. Yang, J., Huo, X., Li, Z., Li, H., Wang, T. and Ma, S. (2023). Study on adsorption and photocatalytic properties of zinc ferrite. Processes 11 : 1607. doi:10.3390/pr11061607

28. Holder, C.F. and Schaak, R.E. (2019). Tutorial on powder X-ray diffraction for characterizing nanoscale materials. ACS Nano 13 : 7359–7365. doi:10.1021/acsnano.9b05157

29. Schneider, C.A., Rasband, W.S. and Eliceiri, K.W. (2012). NIH Image to ImageJ: 25 years of image analysis. Nat. Methods 9 : 671–675. doi:10.1038/nmeth.2089

30. Gritli, I., Chemingui, H., Djebali, K., et al. (2024). Methylene blue adsorption by Fe_3O_4 nanoparticles: an optimization study using response surface methodology. Chem. Eng. Technol. doi:10.1002/ceat.202400006

31. Doan, V.D., Nguyen, N.V., Nguyen, T.L.H., et al. (2023). High-efficient reduction of methylene blue and 4-nitrophenol by silver nanoparticles embedded in magnetic graphene oxide. Environ. Sci. Pollut. Res. 30 : 71543–71553. doi:10.1007/s11356-021-13597-z

32. Arisa, P., Wirawan, T. and Widodo, N.T. (2025). Adsorption of methylene blue using composite Fe_3O_4-ihau fruit peel powder (Dimocarpus longan var. malesianus Leenh.). Indones. J. Chem. Res. 13 : 102–110.

33. Narasimharao, K., Al-Thabaiti, S., Rajor, H.K., Mokhtar, M., Alsheshri, A., Alfaifi, S.Y., Siddiqui, S.I. and Abdulla, N.K. (2022). Fe_3O_4@date seeds powder: a sustainable nanocomposite material for wastewater treatment. J. Mater. Res. Technol. 18 : 3581–3597.

34. Li, M., Dong, C., Guo, C. and Yu, L. (2022). Magnetic activated biochar Fe_3O_4-MOS made from moringa seed shells for the adsorption of methylene blue. Processes 10 : 2720. doi:10.3390/pr10122720

35. Siddiqui, S.I., Alsebaii, N.M., Al-Ghamdi, A.A., et al. (2025). Fe_3O_4/BC for methylene blue removal from water: optimization, thermodynamic, isotherm, and kinetic studies. Materials 18 : 2049. doi:10.3390/ma18092049

36. Lin, W., Huang, Y., Liu, S., Ding, W., Li, H. and Zheng, H. (2024). A novel magnetic nano-adsorbent functionalized with green tea extract and magnesium oxide to remove methylene blue from aqueous solutions: synthesis, characterization, and adsorption behavior. Magnetochemistry 10 : 31. doi:10.3390/magnetochemistry10050031

37. Ho, Y.S. and McKay, G. (1999). Pseudo-second order model for sorption processes. Process Biochem. 34 : 451–465. doi:10.1016/S0032-9592(98)00112-5

38. Revellame, E.D., Fortela, D.L., Sharp, W., Hernandez, R. and Zappi, M.E. (2020). Adsorption kinetic modeling using pseudo-first order and pseudo-second order rate laws: a review. Cleaner Eng. Technol. 1 : 100032. doi:10.1016/j.clet.2020.100032

39. Allafchian, A. and Gharaati, A.R. (2023). Efficient removal of methylene blue from water using magnetic Alyssum homolocarpum seed gum-based matrix. Int. J. Biol. Macromol. 242 : 125027.

40. Kuntubek, A., Kinayat, N., Meiramkulova, K., Poulopoulos, S.G., Bear, J.C. and Inglezakis, V.J. (2020). Catalytic oxidation of methylene blue by use of natural zeolite-based silver and magnetite nanocomposites. Processes 8 : 471.